A Real Time Superresolution Image Enhancement Processor

David R. Gerwe
Boeing Directed Energy Systems, Los Angeles, CA
Paul Menicucci
Boeing Directed Energy Systems, Albuquerque, NM

Abstract

An image processor is discussed that combines many types of image enhancement onto a single compact electronics card. The current enhancements include bad pixel compensation, focal plane array non-uniformity correction, several stages of contrast enhancement, feature sharpening, superresolution, and image motion stabilization. Though there are certainly better algorithms for particular applications, this mixture of algorithms reliably enables the system to substantially improve image quality for a large variety of sensors, platforms, and imaging geometries. The card design hosted an FPGA and microprocessor facilitated rapid development by allowing many complicated algorithm elements to be quickly coded in C, with the FPGA providing horsepower for simpler but more computationally intensive elements. Examples show the quality improvement gained by compensating for image degradations including camera motion, atmospheric turbulence induced blur, focal plane imperfections, camera pixel density, and noise.

1. Introduction

Surveillance imagery commonly suffers from a mix of image degradations including image blur and instability caused by camera pointing motion and atmospheric turbulence, noise effects including photon shot noise, Johnson noise, dark current, faulty pixels, and focal plane non-uniformity, and finally camera pixelization. Image processing methods for mitigating these effects to improve single frame and video image quality are of high value for many applications and has been a prominent subject of research and development [1-24]. This paper focuses on a recently developed hardware system that Boeing has developed called SRTIE (Superresolution Real Time Image Enhancement). SRTIE was developed as an intermediate step toward a real-time Multi-Frame Blind Deconvolution processing system but has been shown to provide strong image quality improvements for a large variety of cameras, platforms, collection geometries, and degradation environments. It has been implemented on a compact electronics board and provides several layers of enhancement:

- Superresolution (pixelization compensation),
- SNR boost,
- Image stabilization,
- Blur compensation and image sharpening,
- Automatic contract enhancement.

This paper is organized as follows. A description of the algorithm is given in Section 2. Section 3 overviews the capabilities of the current hardware prototype. Section 4 provides examples of the application of SRTIE to several video sources. Section 5 concludes with a brief summary of the main points of the paper.

2. SRTIE Algorithm

There are two versions of SRTIE, a software version coded in MatLab and a real time hardware implementation. The MatLab version is more flexible and has a number of features not implemented in the hardware system. However, it can be run in a mode that emulates the hardware calculations exactly by applying appropriate quantization at various points so that the math is performed at the correct bit precision. The algorithm description in this section will apply equally to both systems except where explicitly noted.

The SRTIE system is best characterized as a modular composite of several largely independent enhancement algorithms. Their sequence and interaction is portrayed in Figure 1. The remainder of this section will describe

each module in the order in which they are applied (though it should be noted that in the hardware implementation, independence between some modules is taken advantage allowing their calculations to be performed in parallel).

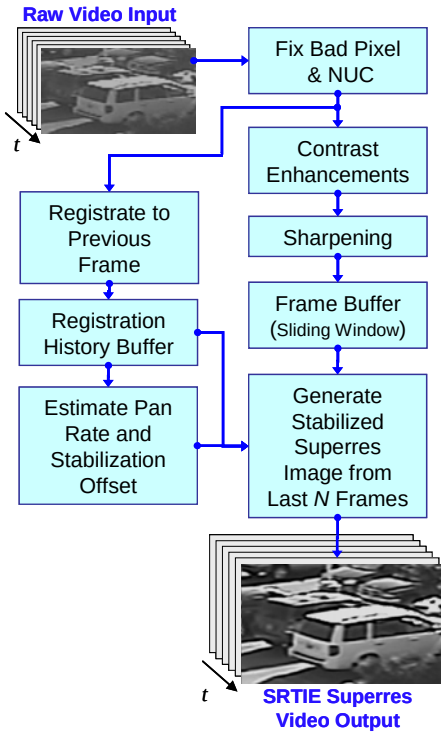

Fig. 1 SRTIE Processing Algorithm

As the image data streams in, a two-point non-uniformity correction (NUC) is performed and bad pixels are replaced by averaging the values of the nearest (non-bad) neighbors. Bad pixel maps and NUC coefficients for each pixel are treated as tables that can be loaded into the MatLab or hardware system for the specific sensor and focal plane array (FPA). Next the data is fed both into a registration calculation module and to the contrast enhancement module. The contrast enhancement module monitors the gray-value statistics of the data and calculates a bias and multiplier defining a linear transformation that is applied to the gray values mapping them such that the central portion of the histogram spans the 12-bit dynamic range that the subsequent calculations are performed at. Values beyond the dynamic range are thresholded. The linear transform coefficients are low-pass filtered to avoid sudden visually disturbing changes and are applied with a one frame lag which eliminates latency that would otherwise be required to read in the full image frame before the necesssary histogram statistics could be obtained. In the hardware version the number of standard deviations of the histogram included in the dynamic range after this linear transformation can be adjusted in real time through a GUI interface. In addition the contrast enhancement model calculates the average brightness gradient across the image and cancels an adjustable fraction of it. This has the benefit of reducing the dynamic range consumed by large spatial scale changes in brightness across the scene due to bright sky background or large scale shadows in the near foreground, preserving it for more interesting fine scale image features.

The output of the contrast enhancement module is fed into the wavelet based sharpening operation that is roughly equivalent to seperating the Fourier spatial-spectrum of the signal into four equal width frequency bands (low, med-low, med-high, and high), boosting or attenuating each independently, and recombining. Boosting the high frequency bands sharpens the image. In the hardware system the boost/attenuation coeffients can be adjusted in real time using sliders on the GUI control interface. The resulting sharpened and contrast enhanced image frame is pushed on to a buffer which holds the last *N* frames (maximum of 12 in the prototype hardware implementation and limited only by memory in the MatLab version). In addition the signal at this point is tapped off to provide one of the output video channels (Figure 3).

Performed in parallel with the constrast and sharpening modules, a registration module determines the translation and rotation values that best align the current frame to the previous frame using a Lucas-Kanade type method [1,25-26]. This registration information is pushed onto a buffer with a depth of 50 frames. A stabilization module determines an instantaneous translational offset to the current displayed output with the following goals:

- Suppress undesirable rapid frame-to-frame jitter motion
- Preserve consistent slower motion from deliberate camera panning
- Prevent large translational differences from building up between the displayed image and camera boresight

The details of the stabilization module are quite involved, so only the basic principles and features will be discussed. Consider the sequence of the frame-to-frame translations output by an idealized perfect registration algorithm that determines the alignment error between each pair of temporally adjacent video frames. The cumulative sum of this sequence corresponds to the pointing motion time history. Shifting the displayed image by this cumulative sum would perfectly counteract any motion and produce a perfectly stablized image. High pass filtering the registration sequence will preserve the rapid jitter components but remove slower motion. Shifting the displayed output by the cummulative sum of the high-pass filtered signal thus suppresses rapid jitter motion and oscillations but preserves deliberate slow panning motion. The filter used in the SRTIE system was based on a proportional-integral-differential (PID) approach which is convenient for real time implementation and can be tuned to adjust the agressiveness with which jitter is suppressed while minimizing undesirable overshoot response associated with

oscillitory motion near the filter resonance or sudden changes in pan direction. An additional exponential decay filter applied to the image display offset prevents buildup of large translational differences due to accumulation of errors in the registration information and slight attenuation of the slow motion components due to imperfect pass-through by the high-pass-filter. A mode selection switch allowed subsets of the stabilization calculations to be chosen:

NoStab - Stabilization module bypassed, no stabilization is performed.
Stare - The registration sequence is not filtered, all motion including slow panning is suppressed.
Pan - Operation is as described in preceding paragraph using filtering of the registration sequence to suppress rapid jitter but preserve slow deliberate camera pan motion.
Auto - This mode estimates and monitors the recent rate of camera pan motion and turns off the high-pass filter if the rate is negligible or falls below the noise level in order to maximimize jitter suppression. In this situation (corresponding to the Stare mode) the exponential decay filter still prevents potential build up of large translational offsets between the raw and displayed frame that can result from small pan motion below the detection threshold.

The superresolution module forms a new output frame by combining the last *N* constrast enhanced and sharpened video frames. The method is less sophisticated than the iterative schemes that are prolifically discussed in the literature [4-9,12-19] but works suprisingly well and is far less computationally demanding. The process is most easily described as follows. Each image is interpolated to a *S*× finer grid, using the information in the registration buffer to align each image to the newest frame. In the current hardware system upsampling is 3× in both horizontal and vertical directions for non-interlaced video, and 4× in vertical and 2× in horizontal for interlaced video. At each pixel location of the fine superresolution grid, the mean and standard deviation of the interpolated values produced from the last *N* video frames are calculated, outliers discarded, and remainders averaged. Values associated with bad-pixel locations in the original data are also discarded before averaging.

3. Real Time Hardware System

The SRTIE algorithm has been implemented on a 3U-CPCI format electronics card that hosts a Virtex 4 FPGA and a Curtiss-Wright SCP124 microprocessor (Fig. 2). This allowed some modules that are highly complex but computationally undemanding like the stabilization calculations to be written in C-code and run on the microprocessor while others that are relatively simple yet require a large number of computations like the bad-pixel replacement and NUC to be performed on the FPGA. Thus this hybrid platform provides a nice mix of processing capabilities that allowed the prototype system to be developed in only 9 months yet achieved a very small footprint. The FPGA furthermore allows the compuations performed by many of the modules to be performed in a pipelined fashion such that the pixel data streams through consecutive modules such that as soon as bad pixel correction is applied to the earlier image lines and columns this data is passed immediately into the circuitry that applies NUC, meanwhile the bad-pixel correction circuitry starts operating on the new image pixel data streaming in. This pipelined application of the algorithmic modules as the pixel data for an image frame streams through the processor continues with the contrast enhancement, wavelet sharpening, and registration modules. This is great importance in achieving low-latency and high frame rates.

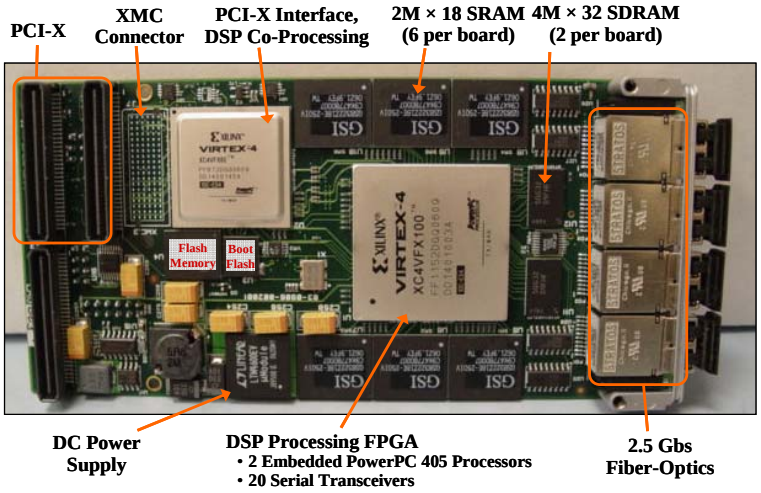

Fig. 2 SRTIE Processor

The SRTIE system is diagramed in Fig. 3. The camera signal is fed into the SRTIE electronic board (here shown in a large rack that contains other supporting diagnostics elements). The output consists of two channels. The first is a video stream at the same frame size and field-of-view (FOV) as the raw input video but with bad-pixel replacement, NUC, contrast enhancement, sharpening, and image stabilization applied. The second channel also has

superresolution applied, but only to a smaller region (currently a 64×64 pixels at the input resolution resulting in a 196×196 output after 3× superresolution). This "region-of-interest" (ROI) is steerable by a joystick, and is outlined on the first full FOV channel. A Java GUI application running on a PC computer communicates to the SRTIE board via an ethernet connection allowing adjustment of the settings for the contrast enhancement, sharpening, and stabilization modules. The current prototype system produces output frames at 14 Hz (skipping input frames as necessary if the input feed is faster than 14 Hz) and with a latency of less than 1/15 sec.

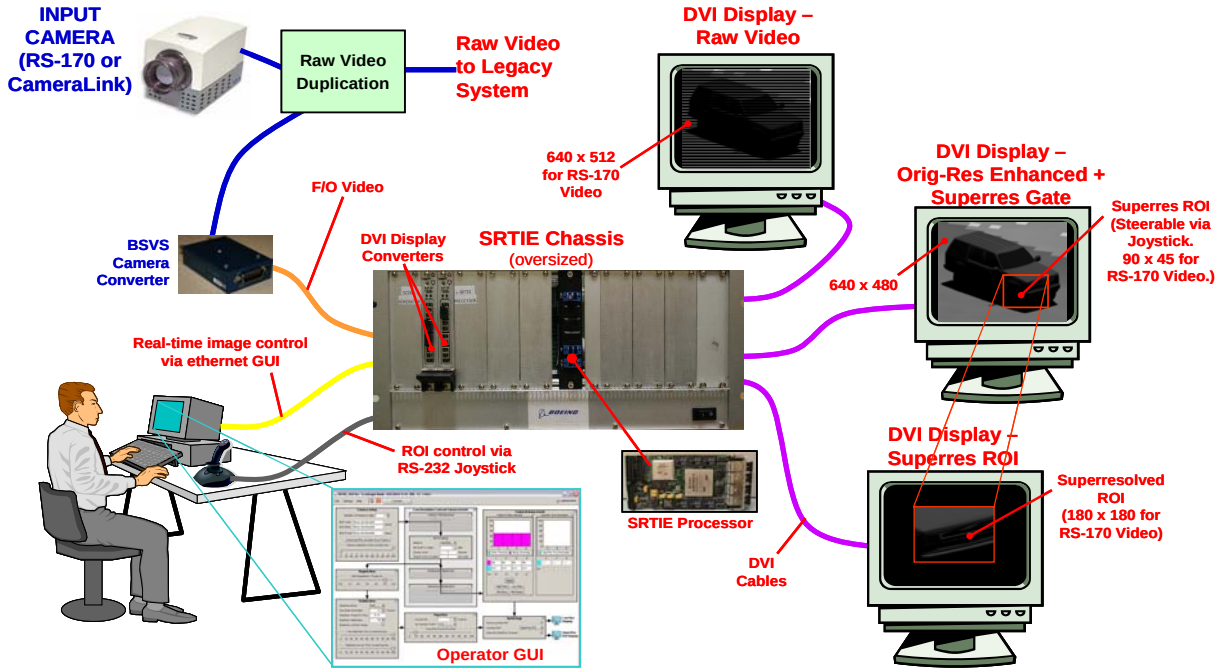

Fig. 3 SRTIE Prototype System

4. Application of SRTIE to Video Data

SRTIE has been applied to video data sets from over 15 different visible and IR camera systems and representing a wide range of environmental conditions, target-platform geometries, and scene content. What has been remarkable is that is has almost always provided a significant improvement to image quality! We attribute this to the fact that it is a tightly coupled composite of several layers of enhancement each targeting a different image quality aspect. The nature of the improvement varies considerable depending on the particular mix of degradations. In many situations a true superresolution effect was observed in which the course pixelization of the original image was quite apparent (e.g. aliasing of sharp edge features was readily apparent) and the output image was of visibly better resolution (Fig. 4-6a). In others the main benefit was blur compensation. And surprisingly, in many systems the largest benefit was the suppression of various noise sources (Fig. 6b-8)! Last the image stabilization feature has worked very well and been recognized as one of the major benefits of the system - unfortunately the benefit to visual quality is best conveyed by viewing the live video, not in a static document format.

Fig. 4. Application of SRTIE to video data captured with a home consumer grade video camera. The middle panel shows the image resulting from 3x upsampled bilinear interpolation of the raw image, which compared to the SRTIE processed output in the right-hand panel clearly shows SRTIE has achieved a strong degree of superresolution.

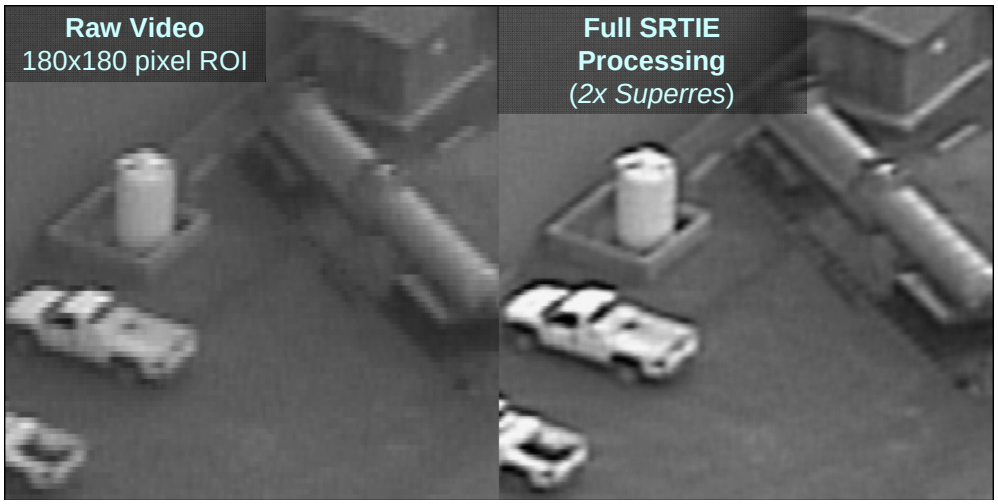

Fig. 5. Application of SRTIE to a live video feed from a visible band camera hosted on a Scan Eagle unmanned air vehicle.

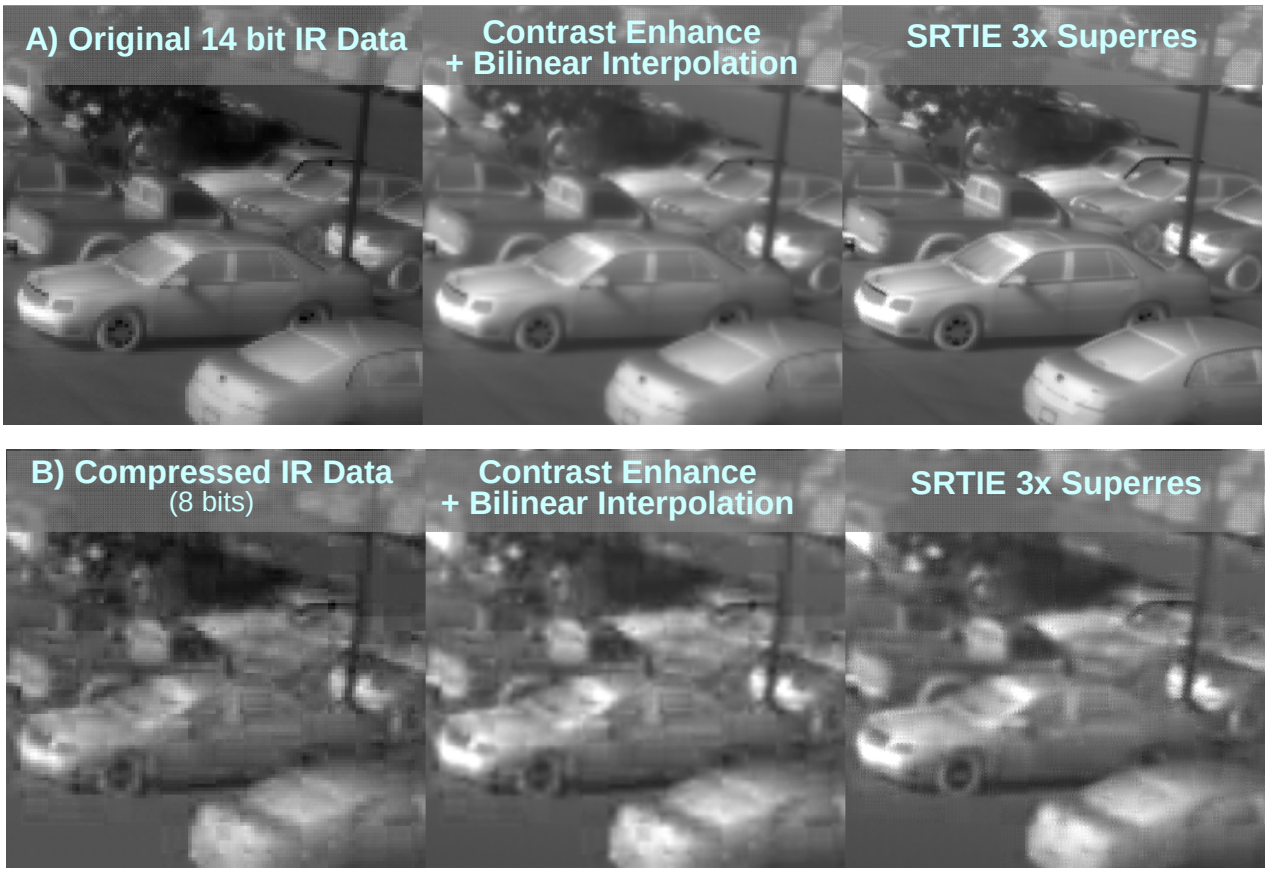

Fig. 6. Application of SRTIE to video data captured with a 14 bit IR camera. The upper row (A) shows processing of the original raw data, while the lower row (B) shows processing of the IR data after MPEG compression. The upper row shows clear evidence of superresolution. SRTIE processing of compressed data is not able to recover the original quality but does strongly suppress compression artifacts.

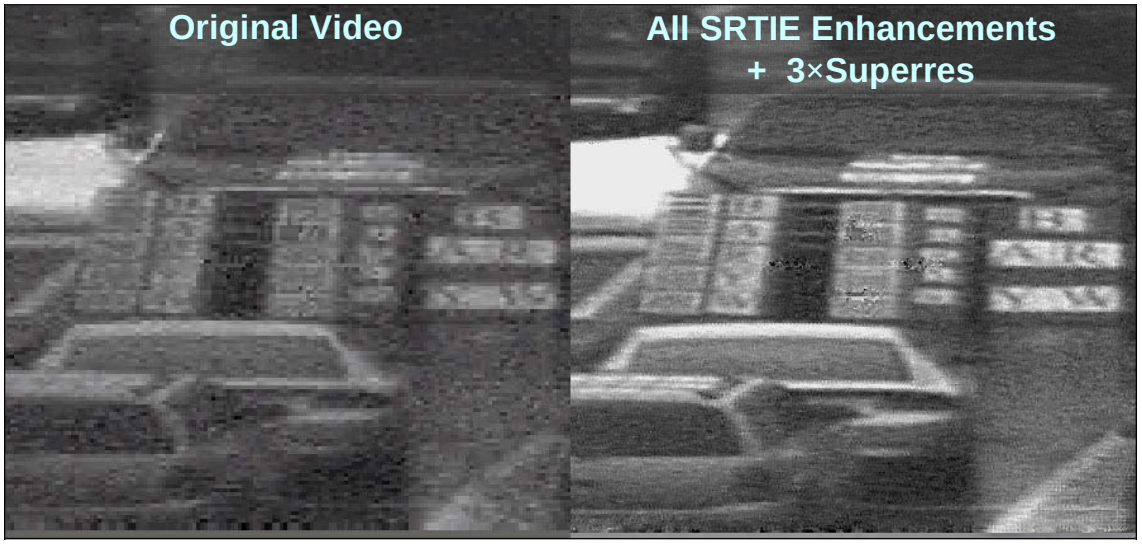

Fig. 7. Application of SRTIE to video data captured with an L3 sensor aboard a flying helicopter. Resolution target boards have been placed in the scene. Several 3-bar targets and letters are much more easily recognizable after SRTIE processing.

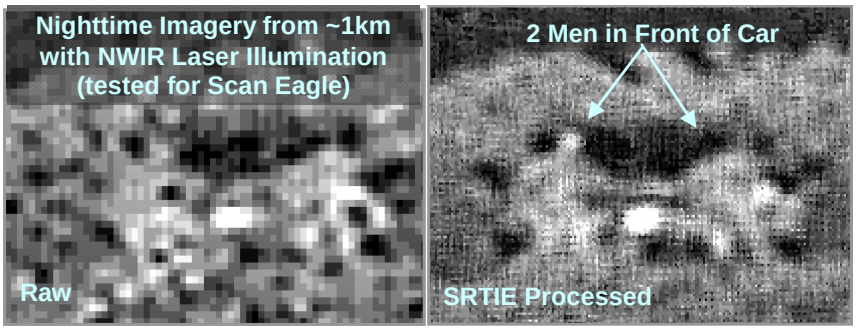

Fig. 8 Application of SRTIE to nightime imagery collected using laser illumination suppresses motion jitter and strong photon and laser speckle noise, significantly increasing ability to recognize two human subjects.

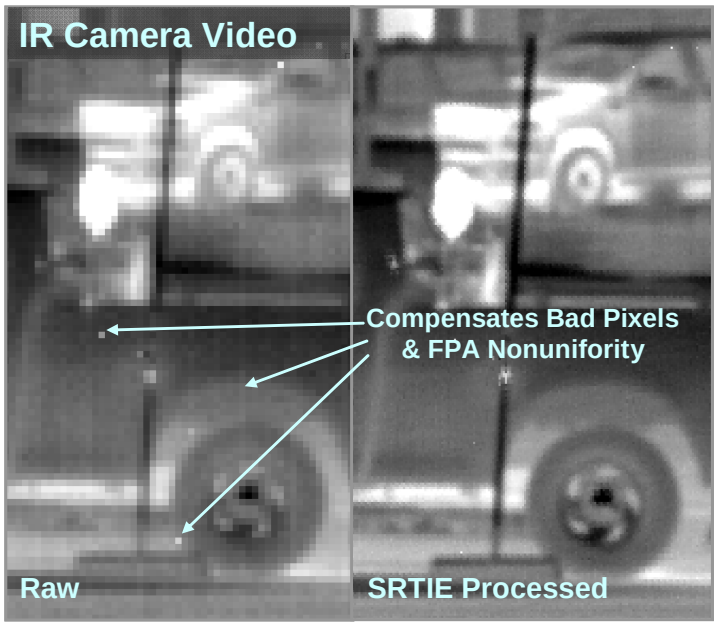

Fig. 9 Application of SRTIE to data collected with an IR camera signficantly improves image resolution through superresolution and sharpening. Also despite the fact that the bad-pixel correction and NUC features of SRTIE were not used here, the multi-frame averaging and outlier rejection features provided strong compensation against these degradations.

5. Summary

Digital superrresolution algorithms are well established and have been widely demonstrated with strong success as non-real-time post processing techniques. This paper presents the implementation of a non-iterative variation in real-time hardware. Furthermore the system incorporates several additional layers of enhancement including automated contrast enhancement, sharpening, and stabilization. As illustrated by the many examples shown in section 4, this composition of algorithms has proven to reliably provide strong visual quality improvement for a wide variety of video image sources and environmental conditions. The current biggest limitation are the artifacts that appear when SRTIE is applied to imagery with internally moving targets[3-4,20]. This is a result of its use of a global motion model in the registration algorithm. Boeing and HRL are working in collaboration to develop updates using more sophisticated motion estimation models and treatments to address this deficit.

6. Acknowledgements

The authors wish to acknowledge Chris Musial and Chris Kiser for their guidance and contributions in developing the registration and sharpening modules. The authors thank L3 Communications Wescam and Insitu for providing video data used in the testing and demonstration of the SRTIE system.

7. **References**

1. R. C. Hardie, K. J. Barnard, *et al*, "High–resolution image reconstruction from a sequence of rotated and translated frames and its application to an infrared imaging system," Opt. Eng. **37**(1) 247-260 (1998).
2. T. R. Tuinstra and R.C. Hardie, "High-resolution image reconstruction from digital video by exploitation of nonglobal motion," Opt. Eng. **38**(5), 806-814 (1999).
3. S. Farsiu, D. Robinson, M. Elad, and P. Milanfar, "Robust shift and add approach to super-resolution," SPIE Proc. **5203,** 121-129 (2003).
4. S. Farsiu, D. Robinson, M. Elad, and P. Milanfar, "Advances and challenges in super-resolution," Wiley Periodicals, Inc., Int J Imaging Syst Technol **14**, 47–57, (2004). Published online in Wiley InterScience (www.interscience.wiley.com). DOI 10.1002/ima.20007.
5. R. Fransens, C. Strecha, and L. V. Gool, "Optical flow based super-resolution: A probabilistic approach," Comp. Vision and Image Understanding **106**, 106-115 (2007).
6. M. Elad and A. Feuer, "Superresolution restoratino of an image sequence: adaptive filtering approach," IEEE Trans. Image Proc. **8**(3), 387-395 (1999).
7. N. Nguyen, P. Milanfar, G. Golub, "Efficient generalized cross-validation with applications to parametric image restoration and resolution enhancement," IEEE Trans. Image Proc. **10**(9), 1299-1308 (2001).
8. D. Fraser, G. Thorpe, and A. Lambert, "Atmospheric turbulence visualization with wide-area motion-blur restoration," **16**(7), 1751-1758 (1999).
9. M. Roggemann, B. M. Welsh, and T. L. Klein, "Algorithm to reduce anisoplanatic effects on infrared images," SPIE Proc. **4125**, 140-149 (2000).
10. M. Roggemann and W. R. Reynolds, "Algorithm Block-matching algorithm for mitigating aliasing effects in undersampled image sequences," Opt. Eng. **41**(2), 359-369 (2002).
11. D. Reddy, Z. Yue, and P. Topiwala, "An efficient real time superresolution ASIC system," Proc. **6957**(09), 1-8 (2008).
12. D. Gerwe, D. Lee, and J. Barchers, "Supersampling Multiframe Blind Deconvolution Resolution Enhancement of Adaptive Optics Compensated Imagery of LEO Satellites," Proc. SPIE 4091, 187-205 (2000).
13. R. C. Puetter, "Pixon® sub-diffraction space imaging," SPIE **7094**(05), 1-12 (2008).
14. B. J. Thelen, D. A. Carrara, and R. G. Paxman, "Fine-resolution imagery of extended objects observed through volume turbulence using phase-diverse speckle," SPIE Proc. **3763**, 102-111 (1999).
15. B. J. Thelen, D. A. Carrara, and R. G. Paxman, "Overcoming turbulence-induced space-variant blur by using phase-diverse speckle," JOSAA **26**(1), 206-218 (2009).
16. J. J. Dolne, P. Menicucci, D. Miccolis, K. Widen, *et al*, "Advanced image processing and wavefront sensing with real-time phase diversity," Appl. Opt. **48**(1) A30-34 (2009).
17. D. C. Dayton, J. D. Gonglewski, and C. St. Arnauld, "Scene Based-Blind Deconvolution in the Presence of Anisoplanatism," SPIE Proc. **7466,** K1-8 (2009).
18. D. C. Dayton and J. D. Gonglewski, "High Resolution Anisoplanatic Imaging from an Airborne Platform," SPIE Proc. **6307**(09),1-8 (2009).
19. C. L. Matson, K. Borelli, *et al*, "Fast and optimal multiframe blind deconvolution algorithm for high-resolution ground-based imaging of space objects," Appl. Opt. **48**(1), A75-A92 (2009).
20. C. J. Carrano and J. M. Brase, "Adapting high-resolution speckle imaging to moving targets and platforms," SPIE Proc. **5409**, 96-105 (2004).
21. F. E. Ortiz, C. J. Carrano, E. J. Kelmelis, and J. P. Durbano, "Special-purpose hardware for real-time compensation of atmospheric effects in long-range imaging," SPIE Proc. **6303**, A1-10 (2006).
22. J. Fanning, J. Miller, J. Park *et al*, „IR system field performance with superresolution," SPIE Proc. **6543**, Z 1-12 (2007).
23. K. Krapels, R. G. Driggers, E. Jacobs *et al*, "Characteristics of infrared imaging systems that benefit from superresolution reconstruction," Appl. Opt. **46**(21), 4594-4603 (2007).
24. R. G. Driggers, K. Krapels, *et al*, "Superresolution performance for undersampled imagers," Opt. Eng. **44**(1) 014002: 1-9, (2005).
25. B. D. Lucas and T. Kanade, "An iterative image registration technique with an application to stereo vision," In International Joint Conference on Artificial Intelligence 674-679 (1981).

26. J. M. Fitts, “Precision Correlation Tracking via Optimal Weighting Functions,” IEEE 1979.